Self-Organized Growth of Nanoparticles on a Surface Patterned by a Buried Dislocation Network

F. Leroy,[1,*] G. Renaud,[2] A. Letoublon,[2] R. Lazzari,[3] C. Mottet,[1] and J. Goniakowski[3]

[1]*CRMCN-CNRS, Campus de Luminy, case 913, 13288 Marseille Cedex 9, France*

[2]*Département de Recherche Fondamentale sur la Matière Condensée SP2M/NRS, CEA-Grenoble, 17, rue des Martyrs, F-38054 Grenoble, France*

[3]*Institut des Nanosciences de Paris, CNRS UMR 7588-Universités Paris VI-VII, 140, rue de Lourmel, 75015 Paris, France*

(Received 30 March 2005; published 26 October 2005)

The self-organized growth of Co nanoparticles is achieved at room temperature on an inhomogenously strained Ag(001) surface arising from an underlying square misfit dislocation network of 10 nm periodicity buried at the interface between a 5 nm-thick Ag film and a MgO(001) substrate. This is revealed by *in situ* grazing-incidence small-angle x-ray scattering. Simulations of the data performed in the distorted wave Born approximation framework demonstrate that the Co clusters grow above the dislocation crossing lines. This is confirmed by molecular dynamic simulations indicating preferential Co adsorption on tensile sites.

DOI: 10.1103/PhysRevLett.95.185501 PACS numbers: 61.46.+w, 61.10.Eq, 61.72.Hh, 68.55.Ac

The fabrication of ordered metal and semiconductor nanoparticles on solid surfaces with uniform and controllable size and shape and with a high spatial density is an important challenge as it may find applications in future nanoelectronics [1], ultrahigh density recording [2], and nanocatalysis [3]. Two different routes have been taken towards nanopatterning: one by developing new scanning techniques with nanometer resolution [4], the other by transferring the periodicity of spontaneous self-organized surface patterns, such as surface reconstructions [5], to nanoparticle superlattices. The latter approach avoids the broadening of the size distribution inherent to the random processes of deposition and diffusion on flat substrates and offers an economic and parallel way to realize high density integration, for which lithography techniques find their limits. The self-organized growth (SOG) of magnetic materials is an appealing technique, for instance, in view of magnetic recording.

It has been predicted that strain patterned substrates induced by a buried dislocation network (DN) can serve as templates for growing uniform and regularly spaced nanostructures [6]. Because of long-range repulsive interactions, the dislocations arrange into highly ordered periodic networks. The inhomogeneous strain field experienced by diffusing adatoms gives rise to heterogeneous nucleation and growth at specific sites, yielding a well-ordered nanoparticle superlattice [7–9]. So far, long-range ordering of nanoparticles has been achieved only for semiconductor quantum dots (see, for instance, [10]), whereas experiments on metals have revealed an ordered growth only below RT on closed packed (111) surfaces of fcc crystals and the dislocations were localized just one monolayer below the surface.

In this Letter, we present a new method based on a (001) metal surface nanostructured by a misfit dislocation network buried few nanometers below the surface. We show that the trapping energy of adatoms is large enough to allow an ordering of nanostructures at RT. The cobalt/silver interface is chosen because it is a test bed for magnetic nanoparticles, as Co exhibits a three-dimensional (3D) growth on Ag(001) and because it does not alloy [11] at RT. To modulate the surface strain field, a Ag film was grown on a MgO(001) substrate. Because of the cube on cube epitaxial relationship and the 3% lattice mismatch between Ag and MgO(001), strain relaxation occurs via a square misfit dislocation network with a period of $D \sim 10$ nm [12].

If scanning tunneling microscopy is the technique of choice to study SOG, it suffers in the present case from its inability to probe the DN internal characteristics. In this context, depth sensitivity as well as statistical information on a macroscopic scale to characterize the order quality are crucial to understand SOG processes. For that reason, we resorted to *in situ* grazing-incidence small-angle x-ray scattering (GISAXS) [13,14], which has become an ubiquitous tool to investigate nanometer scale order close to a surface.

The experiments were carried out at the European Synchrotron Radiation Facility (ESRF), on the BM32 beam line, delivering a monochromatic (0.06888 nm) x-ray beam, and using a newly developed setup allowing performing GISAXS, grazing-incidence x-ray diffraction (GIXD), and x-ray reflectivity (XR) measurements on the same sample, *in situ,* in ultrahigh vacuum (UHV), at different growth stages. The incident x-ray beam impinges on the surface at a grazing angle α_i and the scattered intensity is recorded as a function of out-of-plane angle α_f and in-plane angle $2\theta_f$ [Fig. 2(c)]. These angles allow defining the reciprocal space coordinates $Q_\perp$ and $Q_\parallel$, respectively, perpendicular and parallel to the surface. The small-angle scattering was collected on a one megapixel 16-bit x-ray CCD camera located at $\sim$1.7 m downstream from the sample. The MgO(001) single crystal was prepared following a procedure yielding a high quality surface [15]. Ag

and Co were, respectively, deposited, under UHV (base pressure 5.10^{-11} mbar), using a Knudsen cell and an electron bombardment source while performing GISAXS, GIXD, and XR measurements. The deposition rates were *in situ* calibrated with a quartz microbalance and XR. A 100 nm-thick 2D Ag film was first grown on MgO(001) at RT and then annealed at 900 K, yielding a Ag(001) film of high crystalline quality (mosaic spread smaller than 0.05°) and exhibiting a well-ordered interfacial DN as revealed by many diffraction satellites around the Ag Bragg peaks [12]. Then the film was thinned *in situ* by ion bombardment until ~5 nm thickness (as determined by XR), while the thinning process was monitored by Ag(110) anti-Bragg GIXD measurements (Fig. 1). At 470 K [Fig. 1(b)], a layer by layer ablation mode was used to measure the thinning speed; then the temperature was raised to 570 K [Fig. 1(c)] to stay in a regime of step retraction [16], thus keeping large terraces (100 nm) and low roughness.

Before proceeding to the Co growth, a detailed (nano)-crystallographic study of the strain patterned substrate was performed by GISAXS. Similarly to GIXD experiments, this first step is necessary in order to analyze the GISAXS images which have been measured after Co deposition as interferences between the waves scattered by the substrate and those scattered by the Co nanostructures may occur. Figures 2(a) and 2(b) display two GISAXS images measured on the Ag/MgO(001) film with the incident x-ray beam parallel to the ⟨110⟩ and ⟨100⟩ MgO(001) crystalline axes. Sharp scattering rods in the $Q_{\parallel}$ direction reveal a periodic nanopattern of fourfold symmetry. As the intensity along the scattering rods quickly decreases as a function of $Q_{\perp}$, the GISAXS signal does not arise from a surface superstructure for which the intensity should be flat and extend much farther in $Q_{\perp}$. Therefore, the measured rods are due to the buried DN. As expected [12], the in-plane rod positions correspond to dislocation lines oriented along the ⟨110⟩ substrate directions, with a periodicity $D = 10.95$ nm that matches to a coincidence site lattice of $\Lambda \sim 37$ oxygen atoms of the MgO(001) substrate and 38 (37 + 1) Ag atoms. The two scattering rods for the x-ray beam parallel to the ⟨110⟩ and ⟨100⟩ MgO(001) crystalline axes are thus labeled $(1/\Lambda, 1/\Lambda, L)$ and $(2/\Lambda, 0, L)$, respectively, using MgO(001) reciprocal lattice units. The quality of the dislocation network is revealed by the correlation length of the superlattice $D(Q_{\parallel}/\Delta Q_{\parallel}) = 170$ nm, as deduced from the full width half maximum ($\Delta Q_{\parallel}$) of the scattering rods. A quantitative analysis of the $(1/\Lambda, 1/\Lambda, L)$ and $(2/\Lambda, 0, L)$ scattering rods was performed within the distorted wave Born approximation (DWBA) framework [17] since it provides a characterization of the dilatation field inside the Ag film and the MgO substrate, both parallel and perpendicular to the interface [18]. As expected from the isotropic linear elasticity theory applied to a perfect misfit dislocation network [19], an exponential damping of the dilatation field as a function of the vertical z coordinate was assumed inside the film (Θ_f) and in the

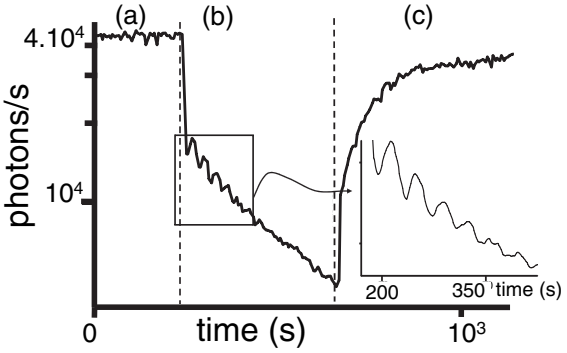

FIG. 1. Ag(110) anti-Bragg peak intensity (logarithmic basis) versus time for different experimental conditions. (a) At 470 K before ion bombardment (IB), the intensity is steady. (b) IB is started and the temperature is kept at 470 K; the intensity decreases and oscillates, exhibiting a layer by layer ablation process (see inset). (c) Keeping IB, the temperature is increased up to 570 K: The intensity increases to reach a steady, maximum value.

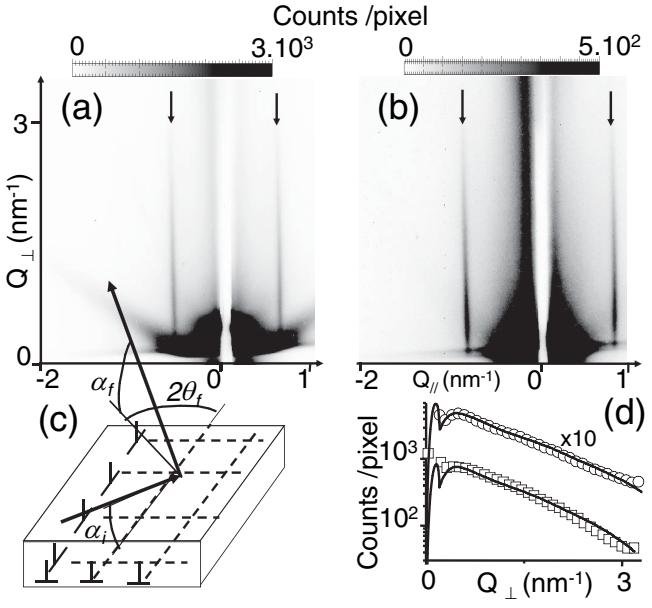

FIG. 2. (a) Experimental GISAXS pattern with the incident beam along the MgO[110] direction. The intensity is represented on a linear scale and the $Q_{\parallel}$ ($Q_{\perp}$) axis ranges from -2 to 1 nm^{-1} (0 to 3.4 nm^{-1}). The direct and reflected beams are hidden by a vertical beamstop. The first order DN scattering rods are indicated by arrows. Inclined rods at 54° with respect to the surface normal arise from Ag(111) facets [present because the Ag films are not perfectly 2D but made of very large flat Ag islands with a top (001) surface and small (111) facets at the edges, as seen by cross section TEM]. (b) Same as (a), but with the incident beam along [100]. (c) Scheme of the scattering geometry of GISAXS. (d) Cuts along $Q_{\perp}$ of the scattering rods of the dislocation network extracted from GISAXS pattern (a) (□) and (b) (○) (multiplied by 10 for clarity) and best fits of λ (solid lines); see Eq. (1).

substrate (Θ_s):

$$\Theta_f = \gamma_f \exp(-z/\lambda) \quad \text{and} \quad \Theta_s = \gamma_s \exp(z/\lambda), \qquad (1)$$

where $z = 0$ at the interface and λ is the attenuation length of the dilatation field associated with the misfit dislocations. The elastic constants of both materials are taken into account through $\gamma_f = 0.015$ and $\gamma_s = -0.011$ [19]. For both $(1/\Lambda, 1/\Lambda, L)$ and $(2/\Lambda, 0, L)$ scattering rods, a fit of λ equal to 1.05 nm [Fig. 2(d)] was deduced as qualitatively expected [19].

GISAXS measurements were then performed during the growth of Co on this nanostructured template for different substrate temperatures and Co growth rate. Co was finally deposited at room temperature and at a very low rate (4×10^{-3} nm/min), respectively, to decrease the thermal energy of the adatoms with respect to the DN nucleation trapping potential [5] and to increase the diffusion length of Co atoms and, thus, their probability to find a nucleation site. No ordering of Co clusters was found at higher temperatures or deposition rates. From the very beginning of the growth (0.04 nm), the subtracted GISAXS images (after and before Co deposition) display intensity oscillations along the DN scattering rods with a damped sinusoidal shape [20] [Fig. 3(a)]. The oscillation amplitude increases with deposition time, reaches a maximum for an equivalent Co deposited thickness of 0.19 nm, and then decreases [Fig. 3(b)]. The period, equal to 5 nm, is a signature of the height difference between the Co clusters and the interfacial DN. Most importantly, these oscillations reveal the SOG of Co clusters, since an interference effect can occur only if the phase shift between the waves scattered by the Co clusters and those scattered by the DN is well defined, i.e., if the Co clusters are well localized with respect to the dislocation positions. Indeed, the intensity is the sum of three terms: the intensity scattered by the DN, the one scattered by the Co islands, and the interference term between both:

$$I = |F_{\mathrm{DN}}|^2 + |F_{\mathrm{Co}}|^2 + 2F_{\mathrm{DN}}F_{\mathrm{Co}} \cos(\vec{Q}_{\parallel} \cdot \vec{d}_{\parallel} + Q_{\perp} d_{\perp}), \qquad (2)$$

where F_{DN} (F_{Co}) is the form factor of the DN (the Co clusters), i.e., the Fourier transform of the dilatation field of the DN (of the shape of the Co clusters), and $\vec{d}_{\parallel}$ and $d_{\perp}$ are the parallel and perpendicular coordinates, respectively, of the Co clusters with respect to the dislocation crossing lines [Fig. 3(c)].

The very small intensity of the oscillations with respect to the rods before Co deposition (i.e., $|F_{\mathrm{DN}}|^2$) shows that $|F_{\mathrm{Co}}| \ll |F_{\mathrm{DN}}|$. Hence, the $|F_{\mathrm{Co}}|^2$ term can be neglected in Eq. (2). Thus, the interference term, which contains the information on the Co clusters location, is simply obtained by the subtraction of GISAXS measurements after and before Co deposition. On the basis of the strain field symmetries, two high-symmetry sites are possible for the Co clusters: above the dislocation crossing lines or in between. In order to discriminate between the two possible positions, the interference effect along the $(1/\Lambda, 1/\Lambda, L)$ rod was simulated in the DWBA framework. The Co clusters were taken as cylinders whose height is an integer number of Co atomic layers (AL). The best fit was unambiguously obtained for the clusters located above the dislocation crossing lines [Fig. 3(b)] and a height of 2 AL.

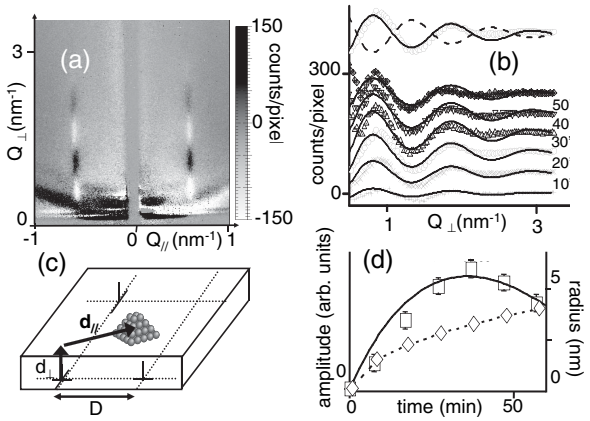

FIG. 3. (a) Experimental interference pattern (after subtraction of the substrate's one) with the incident beam along the [110] direction, for a 0.14 nm-thick Co deposition. The intensity is represented on a linear scale; the $Q_{\parallel}$ ($Q_{\perp}$) axis ranges from -1 to 1 nm^{-1} (0 to 3.26 nm^{-1}). Oscillations along the rods are clearly visible. (b) Intensity of the interference term versus $Q_{\perp}$, for different deposition times (symbols) with best fits (see text). A vertical translation proportional to the time of deposition has been introduced for clarity. Last (top) curve: Interference term (circle) and best fit (solid line) for 0.14 nm-thick Co deposition and a simulated interference term (dashed line) for Co clusters located at the center of the unit cell. (c) Schematic representation of the Co clusters position with respect to the dislocation intersection lines. (d) Oscillation amplitude versus time. Experimental data (□) and best fit (solid line) for the $(1/\Lambda, 1/\Lambda, L)$ DN rod as well as simulated curve of Co clusters radius versus time (short-dashed lines and ◇) for 2 AL high clusters.

To interpret this result, theoretical calculations of the adsorption energy of a Co atom on a nanostructured thin film of Ag(001) on MgO(001) were performed. The energetic model is based on a semiempirical tight binding potential for metal-metal interactions and on a potential fitted to *ab initio* calculations for the metal-MgO(001) ones (details are given in Ref. [21]). The bare strained thin film of Ag(001) on MgO(001) was first investigated. Molecular dynamic simulations were performed on Ag atoms, whereas the oxide surface was frozen. Assuming periodic boundary conditions, the simulations were made on a superlattice unit cell with a lateral periodicity of 9.82 nm ($\Lambda \sim 34$ atoms) and a thickness of 5 nm (24 AL). The adsorption site of Ag was located on top of the O as demonstrated elsewhere [22]. Simulations clearly show that the Ag surface exhibits alternating tensile and compressive areas (Fig. 4), the former being located on top of the dislocations crossing. The Co adsorption on top of the

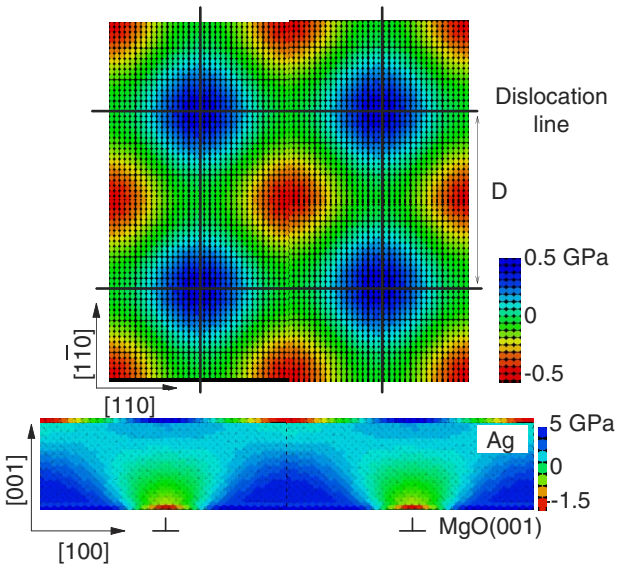

FIG. 4 (color online). Top view (top panel) and side view in the (010) plane (bottom) of the atomic stress map of the Ag nanostructured film. Color code from red/dark to blue/light corresponds to compressive to tensile atomic sites. Because of its exponential decay, the stress field at the top surface is barely visible, and, hence, a different color scale has been used.

tensile zones is found more favorable than on compressive ones with an energy difference of 70 meV. Moreover, the diffusion barrier by hopping is found to be significantly lower on compressive sites as compared to tensile ones (by 60 meV). Such results are comparable to other calculations performed on Pt(111) strained surfaces [23]. We show here that, taking into account a realistic strained surface [the silver film nanostructured by the buried DN on MgO(100) substrate], the energy difference between the adsorption sites is much higher than the thermal activation energy available at room temperature. If we suppose that the first atom adsorption is a good indicator for cluster nucleation [23], such energy difference should contribute to the cluster organization.

The position of Co clusters being determined, we resorted to a detailed analysis of the amplitude of the interference term as function of deposition time. From Eq. (2), the amplitude is proportional to F_{Co}. Assuming a cylindrical shape and a radius R proportional to the square root of time to account for the linear increase of volume during deposition, while the height is kept fixed at 2 AL, the amplitude evolution is in good agreement with the one expected from the measured deposition rate [Figs. 3(b) and 3(c)]. The linear increase of the amplitude at the beginning of the growth is a consequence of the small island size: The damping of the Co form factor with momentum transfer can be neglected and the resulting amplitude is proportional to the island volume, i.e., to the deposition time. The decreasing amplitude at the end of the deposition is due to Co clusters getting closer to coalescence for which the intensity should decrease to zero.

To conclude, we have shown that the periodic surface strain field induced by a misfit dislocation network buried as far as 5 nm below a Ag(001) surface allows controlling the growth of Co clusters at RT, leading to self-organized growth. This result is supported by molecular dynamic simulations. We believe that this method could be used for many different systems, metal thin films being favored with respect to semiconductor ones because of the dislocation mobility necessary to reach the equilibrium state.

We acknowledge the invaluable help of Marion Ducruet and Ameline Crémona for the many sample preparations and of Tobias Schülli during some measurements, as well as the ESRF and BM32 staff for beam availability.

*Electronic address: leroy@crmcn.univ-mrs.fr

[1] A. O. Orlov *et al.*, Science **277**, 928 (1997).
[2] S. Sun *et al.*, Science **287**, 1989 (2000).
[3] M. Valden, X. Lai, and D. W. Goodman, Science **281**, 1647 (1998).
[4] D. Eiglet and E. Schweizer, Nature (London) **344**, 524 (1990).
[5] H. Brune, Surf. Sci. Rep. **31**, 125 (1998).
[6] A. Bourret, Surf. Sci. **432**, 37 (1999).
[7] H. Brune *et al.*, Nature (London) **394**, 451 (1998).
[8] B. Voigtländer and N. Theuerkauf, Surf. Sci. **461**, L575 (2000).
[9] S. Y. Shiryaev *et al.*, Phys. Rev. Lett. **78**, 503 (1997).
[10] J. Stangl *et al.*, Mater. Sci. Eng., C **19**, 349 (2002).
[11] B. Degroote, J. Dekoster, and G. Langouche, Surf. Sci. **452**, 172 (2000).
[12] G. Renaud, P. Guénard, and A. Barbier, Phys. Rev. B **58**, 7310 (1998).
[13] J. R. Levine *et al.*, J. Appl. Crystallogr. **22**, 528 (1989).
[14] G. Renaud *et al.*, Science **300**, 1416 (2003).
[15] O. Robach, G. Renaud, and A. Barbier, Surf. Sci. **401**, 227 (1998).
[16] C. Boragno *et al.*, Phys. Rev. B **65**, 153406 (2002).
[17] S. K. Sinha *et al.*, Phys. Rev. B **38**, 2297 (1988).
[18] A. Seeger, J. Appl. Phys. **30**, 629 (1959). GISAXS is sensitive only to the electronic density contrast. Therefore, it depends only on the dilatation field, i.e., the trace of the strain tensor ($\Theta = \varepsilon_{xx} + \varepsilon_{yy} + \varepsilon_{zz}$).
[19] R. Bonnet and J. L. Verger-Gaugry, Philos. Mag. A **66**, 849 (1992).
[20] The damping is actually due to the curvature of the Ewald's sphere.
[21] A. Ouahab, C. Mottet, and J. Goniakowski, Phys. Rev. B **72**, 035421 (2005).
[22] O. Robach, G. Renaud, and A. Barbier, Phys. Rev. B **60**, 5858 (1999).
[23] R. F. Sabiryanov *et al.*, Phys. Rev. B **67**, 125412 (2003).